

Joule heating and the thermal conductivity of a two-dimensional electron gas at cryogenic temperatures studied by modified 3ω method

Akira Endo,^{a)} Shingo Katsumoto, and Yasuhiro Iye

The Institute for Solid State Physics, The University of Tokyo, 5-1-5 Kashiwanoha, Kashiwa, Chiba 277-8581, Japan

(Dated: 14 September 2022)

During the standard ac lock-in measurement of the resistance of a two-dimensional electron gas (2DEG) applying an ac current $I = \sqrt{2}I_0 \sin(\omega t)$, the electron temperature T_e oscillates with the angular frequency 2ω due to the Joule heating $\propto I^2$. We have shown that the highest (T_H) and the lowest (T_L) temperatures during a cycle of the oscillations can be deduced, at cryogenic temperatures, exploiting the third-harmonic (3ω) component of the voltage drop generated by the ac current I and employing the amplitude of the Shubnikov-de Haas oscillations as the measure of T_e . The temperatures T_H and T_L thus obtained allow us to roughly evaluate the thermal conductivity κ_{xx} of the 2DEG via the modified 3ω method, in which the method originally devised for bulk materials is modified to be applicable to a 2DEG embedded in a semiconductor wafer. κ_{xx} thus deduced is found to be consistent with the Wiedemann-Franz law. The method provides a convenient way to access κ_{xx} using only a standard Hall-bar device and the simple experimental setup for the resistance measurement.

I. INTRODUCTION

Varieties of techniques have been employed for thermometry required to probe the thermal or thermoelectric properties of a two-dimensional electron gas (2DEG) at cryogenic temperatures. For instance, thermopower across a quantum point contact (QPC)¹ or the width of the Coulomb blockade peak at a quantum dot (QD)² has been used to measure the electron temperature T_e of the 2DEG to which the QPC or QD is attached. These techniques require the sophisticated device (QPC or QD) to be fabricated, employing electron-beam lithography, onto the semiconductor wafer harboring the 2DEG. A simpler way is to make use of the resistance of the 2DEG itself. In principle, any aspect of the resistance that depends on the temperature can be used as the thermometer. The resistance at the zero³⁻⁵ or a small (non-quantizing)⁶⁻⁸ magnetic field, negative magnetoresistance due to the weak localization,^{6,7} the amplitude of the Shubnikov-de Haas oscillations (SdHOs),^{9,10} the maximum slope of the Hall resistance between two adjacent integer quantum Hall plateaus,¹¹ activated behavior of a fragile fractional quantum Hall state¹² are among the temperature-dependent phenomena in the resistance that have been used as the thermometer.

For a three-dimensional (3D) bulk material, an interesting ac measurement technique, dubbed the 3ω method,¹³ is known as a method to measure the thermal conductivity. In this method, resistance of a thin and long metallic film deposited on the surface of a 3D sample to be measured is exploited as both the heater and the thermometer. The temperature oscillations ΔT generated by an ac heating current with the angular frequency ω are monitored by detecting the third-harmonic

(3ω) component of the resulting voltage drop (see Sec. II for the basic principles). Owing to the cylindrical decay in the 3D sample of ΔT with the distance r from the wire-like metallic heater,¹⁴ the thermal conductivity can be extracted either from the $\ln\omega$ dependence of the real part (in-phase oscillations) or from virtually ω -independent imaginary part (out-of-phase oscillations) of ΔT .¹³

In the present study, we make an attempt to apply the 3ω method to a 2DEG at cryogenic temperatures, using a Hall-bar device fabricated from a conventional GaAs/AlGaAs wafer hosting a high-mobility 2DEG. The main channel of the Hall-bar device serves simultaneously as the heater and the thermometer. By passing a relatively large ac current I with the angular frequency ω along the main channel, the electron temperature T_e is raised and oscillates with 2ω due to the Joule heating $\propto I^2$. Note that T_e readily becomes higher than the lattice temperature T_p of the GaAs crystal hosting the 2DEG due to the weak electron-phonon coupling at low temperatures in this system.¹⁵ This *current heating technique* has been widely used for the measurement of the diffusion thermopower,¹⁶⁻¹⁸ in which the 2ω component representing the voltage induced by the temperature gradient is detected. In the measurement of the thermopower, however, it suffices to know the time-average of the raised T_e . The oscillations of T_e with time have therefore not been paid attention it deserves thus far, on which we shed light in the present paper. We demonstrate that the highest (T_H) and the lowest (T_L) values of T_e during a cycle of the oscillations can be deduced by measuring the 3ω component of the resistance along the main channel, and then converting the resistance to the temperature via the amplitude of the SdHOs at relatively small magnetic fields. We obtain T_H and T_L for various values of the heating current I . With these temperatures, we further deduce the thermal conductivity of the 2DEG. In this procedure, considerable modification

^{a)} akrendo@issp.u-tokyo.ac.jp

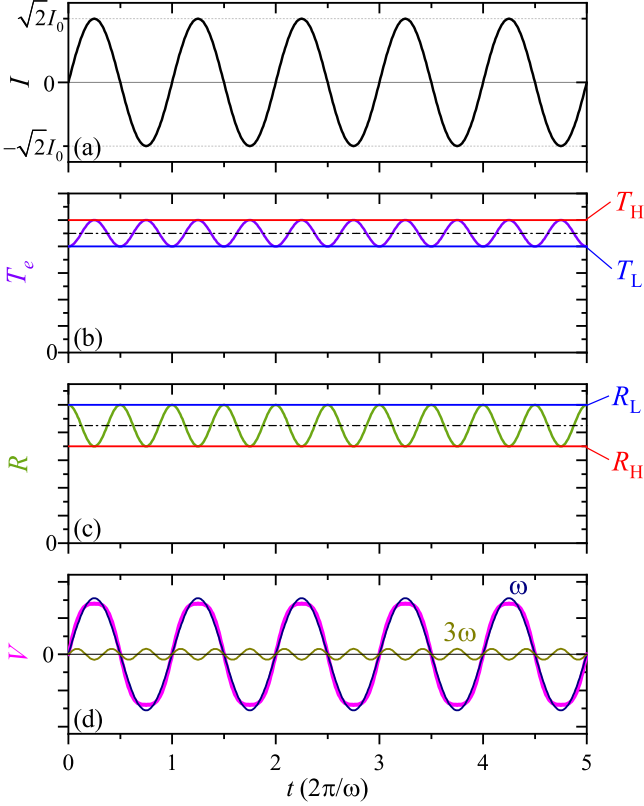


FIG. 1. Schematic diagrams depicting the sinusoidal oscillations of (a) the heating current I , and the resulting oscillations in (b) the electron temperature T_e , (c) the resistance R , and (d) the voltage drop $V = RI$. T_L and T_H represent the lowest and the highest temperatures during a cycle, and R_L and R_H are the resistances at T_L and T_H , respectively. $dR/dT_e < 0$ is assumed in this example. The ω and 3ω components, V_ω and $V_{3\omega}$, contained in V are also plotted with thin lines in (d).

from the original 3ω method is required due to the differing dimensionality and the heat transfer from the 2DEG to the lattice. The thermal conductivity of the 2DEG is obtained at a fixed ω from the thermal flux flowing from the main channel to the electrical contacts through the 2DEG in the voltage arms. The high Hall angle approaching $\pi/2$, achieved with a small magnetic field in a high-mobility 2DEG, substantially simplifies the calculation of the thermal flux. The modified 3ω method described in this paper presents an experimental method to probe the temperature oscillations of a 2DEG due to the Joule heating by an ac current, as well as a convenient way to roughly evaluate the thermal conductivity in the magnetic field, using only a standard Hall-bar device and the experimental setup for the standard ac lock-in resistance measurement.

II. BASIC PRINCIPLES

We start by outlining the basic principles of monitoring the Joule heating by detecting the third harmonics of the resistance. As in the case in the standard ac lock-in measurement of the resistance, we apply an ac excitation current

$$I = \sqrt{2}I_0 \sin(\omega t), \quad (1)$$

with the angular frequency ω [Fig. 1(a)] to the Hall-bar device. To achieve the heating, the rms amplitude I_0 of the current is allowed to take a relatively large value (up to several μA in a Hall-bar device of a GaAs/AlGaAs 2DEG with the width of $\sim 50 \mu\text{m}$). In ordinary resistance measurements at cryogenic temperatures, by contrast, I_0 is kept small (typically $I_0 \lesssim 100 \text{ nA}$) to avoid the heating. Due to the Joule heating $\propto I^2$, the electron temperature T_e of the 2DEG oscillates with the angular frequency 2ω between the lowest (T_L) and the highest (T_H) values [Fig. 1(b)]. If the resistance depends on the temperature, the resistance $R(T_e)$ also oscillates with 2ω between $R_L \equiv R(T_L)$ and $R_H \equiv R(T_H)$ [Fig. 1(c)]. The temperature and the resistance oscillations are approximated well by sinusoidal waves

$$T_e = T_L + (T_H - T_L) \frac{1 - \cos(2\omega t)}{2} \quad (2)$$

and

$$R = R_L + (R_H - R_L) \frac{1 - \cos(2\omega t)}{2} \quad (3)$$

respectively, when the relative variations are small, i.e., $T_H - T_L \ll T_{\text{ave}} \equiv (T_H + T_L)/2$ and $|R_H - R_L| \ll R_{\text{ave}} \equiv (R_H + R_L)/2$.¹⁹ From Eqs. (1) and (3), we can see that the voltage drop

$$V = RI = \sqrt{2}V_\omega \sin(\omega t) + \sqrt{2}V_{3\omega} \sin(3\omega t) \quad (4)$$

contains the fundamental (ω) and the third-harmonic (3ω) components [Fig. 1(d)], where

$$\frac{V_\omega}{I_0} = \frac{3R_H + R_L}{4} \equiv R_\omega, \quad (5a)$$

$$\frac{V_{3\omega}}{I_0} = -\frac{R_H - R_L}{4} \equiv R_{3\omega}. \quad (5b)$$

Therefore, by picking out the ω and the 3ω components V_ω and $V_{3\omega}$ of the (rms) voltage drop employing the lock-in technique, we can deduce the resistance at the lowest and the highest temperatures during the course of the temperature oscillations, given by

$$R_L = R_\omega + 3R_{3\omega}, \quad (6a)$$

$$R_H = R_\omega - R_{3\omega}. \quad (6b)$$

R_L and R_H thus obtained can further be translated to T_L and T_H if the temperature dependence $R(T)$ is known.

In the present study, we employ the temperature dependence of the amplitude of the Shubnikov-de Haas oscillations (SdHOs) for the resistance-to-temperature conversion. As we will show in Sec. IIID, the temperature response to the Joule heating thus deduced, combined with the estimation of the power transferred to the lattice of the GaAs substrate hosting the 2DEG, enables us to evaluate the thermal conductivity of the 2DEG.

III. EXPERIMENTAL RESULTS AND DISCUSSION

A. Experimental details

The Hall-bar device used in the present study was fabricated by standard photo-lithography from a conventional GaAs/AlGaAs wafer containing a 2DEG with the mobility $\mu = 110 \text{ m}^2/(\text{V s})$ and the carrier density $n_e = 2.8 \times 10^{15} \text{ m}^{-2}$ just below the heterointerface at the depth of 70 nm from the surface. The measurements were carried out in a dilution refrigerator (Kelvinox TLM, Oxford Instruments), with the Hall-bar device immersed in the mixing chamber of the fridge. The ω component (V_ω) and the 3ω component ($V_{3\omega}$) were measured simultaneously using two separate lock-in amplifiers (LI-575, NF Corporation). We performed the measurements with the frequency $f = \omega/(2\pi)$ ranging from 19 to 93 Hz and found that the results are virtually independent of f in this frequency range.²⁰ In what follows, we present the data taken with $f = 73 \text{ Hz}$ at the bath temperature $T_{\text{bath}} = 15 \text{ mK}$. (Data taken at other values of f and T_{bath} are presented in the supplementary material.)

B. Dependence of the third harmonics on the heating current

In Fig. 2, we plot R_ω and $R_{3\omega}$ given by Eq. (5) obtained from V_ω and $V_{3\omega}$ measured with the lock-in amplifiers for various values of I_0 ranging from 10 nA to 5 μA . R_ω is nothing but the resistance obtained by ordinary ac lock-in measurement. It exhibits SdHOs which develop, with the increase of the magnetic field B , into the quantum Hall effect (QHE) state characterized by the flat areas of $R_\omega = 0$ having a finite magnetic-field span [Fig. 2(a)]. Only spin-unresolved even-integer QHE states are observed in the magnetic-field range shown in the figure. [The Landau-level filling factor $\nu = n_e h/(eB)$ is shown by the top axis.] Following the increase in I_0 , the amplitude of SdHOs diminishes and the flat areas of QHE shrinks toward the center. As is well known, these behaviors are attributable to the raised electron temperature due to the Joule heating. Our interest in the present study is mainly on the behavior of $R_{3\omega}$ representing the decrement (multiplied by 1/4) of the resistance, while the temperature varies from the lowest (T_L) to the highest (T_H) values within a cycle [Eq. (5b)]. As can be seen in Fig. 2(b), the Joule heating is apparently not enough

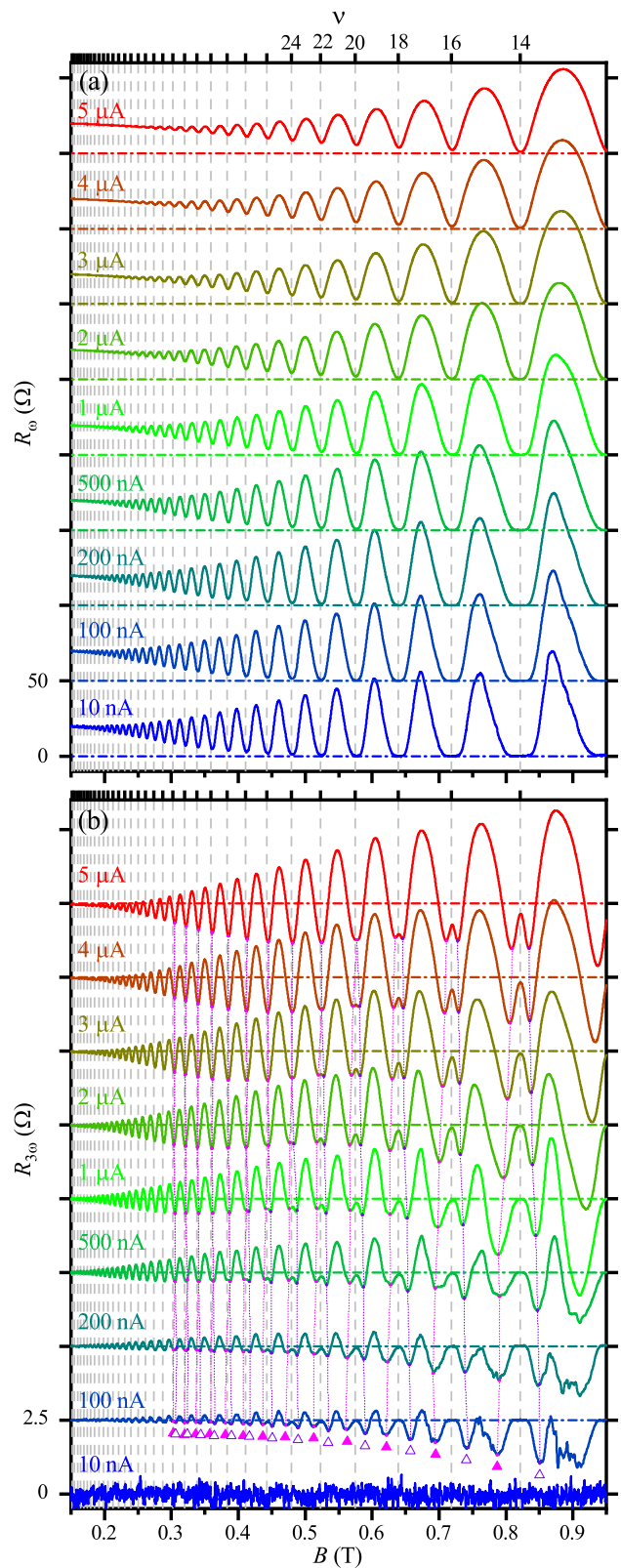


FIG. 2. The ω (a) and 3ω (b) components of the resistance R_ω and $R_{3\omega}$ for various values of the heating current I_0 noted in the figures. Traces are sequentially offset by 50 and 2.5 Ω in (a) and (b), respectively, for clarity, with increasing I_0 . The vertical dashed lines and the horizontal dotted-dashed lines indicate the positions of the even-integer fillings (top axis) and the zero for the corresponding trace, respectively. See the text for the upward triangles accompanied by dotted lines in (b).

to generate the temperature oscillations detectable with $R_{3\omega}$ at $I_0 = 10$ nA. Oscillations in $R_{3\omega}$ become apparent at $I_0 = 100$ nA and the amplitude initially increases with I_0 reflecting the increase in $\Delta T = T_H - T_L$. With further increase in I_0 , however, the amplitude starts to decline, gradually from the lower B side.²¹ This is because the effect of increasing ΔT becomes overridden by the decrease in the amplitude of SdHOs with the increase in T_{ave} , and the declination is more prominent for a lower B . At low B , $R_{3\omega}$ exhibits oscillations in phase with those of R_ω . This indicates that the decrement in the resistance by ΔT takes a local maximum and a local minimum at the peaks and the troughs of the resistance, respectively, resulting in the diminished amplitude of the SdHOs. The locations of the peaks remain the same between $R_{3\omega}$ and R_ω up to higher B , consistent with the decreasing resistance with ΔT at the peaks. In the vicinity of minima in R_ω , by contrast, $R_{3\omega}$ takes on rather complicated line shape at higher B . The flat areas of $R_{3\omega} = 0$ appear at the locations corresponding to $R_\omega = 0$ areas at high- B and low- I_0 regions, where the QHE is robust and hardly affected by ΔT . Two minima flanking a flat area are seen, which represent the increase in the resistance caused by ΔT in the region adjacent to the flat area leading to the shrinking of the flat area. The minima on the higher-field (lower-field) side of a flat area are indicated by open (solid) upward triangles for $I_0 = 100$ nA, and the accompanying dotted lines are eye-guides to follow the shift of the minima with increasing I_0 . With the decrease of B and/or increase of I_0 , the two minima get close to each other narrowing the flat area, thereby generating the line shape containing alternating high and low peaks. The two minima eventually merge and engulf the flat region, signaling the transition from QHE to SdHOs. Note that the peculiar line shape in $R_{3\omega}$ with alternating peak heights survives down to the B -range where QHE is not apparent in R_ω ($0.3 \lesssim B \lesssim 0.5$ T for $I_0 = 100$ nA and 200 nA), revealing the presence of the precursor of the QHE state in these regions.

C. Response of the electron temperature to the Joule heating

In this section, we deduce the lowest (T_L) and the highest (T_H) temperatures for various I_0 from the measured R_ω and $R_{3\omega}$ shown in Sec. IIIB. The procedure is illustrated in Fig. 3, taking the case for $I_0 = 1$ μ A as an example. The first step is to transform R_ω and $R_{3\omega}$ [Fig. 3(a)] into R_L and R_H , the resistances of the 2DEG device at the moments when the electron temperatures are T_L and T_H , respectively, using Eq. (6). The resulting R_L and R_H are shown in Fig. 3(b). They exhibit SdHOs with differing amplitudes, reflecting the difference in the temperature.

The next step is to deduce T_L and T_H from R_L and R_H . To this end, we employ the well-known temperature and magnetic-field dependence of the amplitude δR_{amp}

of the SdHOs²²,

$$\frac{\delta R_{\text{amp}}}{4R_0} = \exp\left(-\frac{\pi}{\mu_q B}\right) A\left(\frac{T_e}{T_c}\right), \quad (7)$$

for the resistance-to-temperature conversion, where $A(x) \equiv x/\sinh x$, $T_c \equiv \hbar\omega_c/(2\pi^2 k_B)$ with $\omega_c = eB/m^*$ being the cyclotron angular frequency and m^* being the effective mass, R_0 is the resistance at $B = 0$, and μ_q represents the quantum mobility. The first and the second factors represent the damping of the amplitude by the impurity scattering and the temperature, respectively. In order to apply Eq. (7), we need to extract the amplitude of the SdHOs from R_L and R_H . This is done by the method we used to extract the oscillatory component detailed in a previous publication²³: briefly, upper and lower envelope curves R_{up} and R_{lw} are defined as spline curves smoothly connecting the maxima and minima, respectively, and with them we obtain the slowly-varying background $R_{\text{bg}} = (R_{\text{up}} + R_{\text{lw}})/2$, the oscillatory part $\delta R = R - R_{\text{bg}}$, and the amplitude $\delta R_{\text{amp}} = (R_{\text{up}} - R_{\text{lw}})/2$. The oscillatory parts δR_L and δR_H contained in R_L and R_H , respectively, extracted by this procedure are plotted in Fig. 3(c).

The value of μ_q in Eq. (7) is determined from R_ω at $I_0 = 10$ nA. [Details of the procedure is presented in the supplementary material IV.] At this current, the Joule heating is negligibly small [$R_{3\omega} \simeq 0$, see Fig. 2(b), and thus $R_L \simeq R_H \simeq R_\omega$] and T_e is expected to be close to the bath temperature $T_{\text{bath}} = 15$ mK.²⁴ We extract δR_{amp} from R_ω following the procedure described above. Substituting $T_e = T_{\text{bath}}$ and using μ_q as a fitting parameter, we search for the value of μ_q with which Eq. (7) reproduces the B -dependence of δR_{amp} . [This is basically the same as the well-known method using the Dingle plot.²²] We find that excellent agreement is achieved for $B \lesssim 0.35$ T with $\mu_q = 4.1$ m²/(V s). Slight deviation at higher magnetic fields [Fig. S6 (b) in the supplementary material] is attributable to the onset of the spin-splitting. Although spin-resolved odd-integer QHE states are not observed in the magnetic-field range examined in the present paper as mentioned in Sec. IIIB, the commencement of incomplete spin splitting is known to reduce the peak height of the SdHOs,²⁵ leading to the deviation from Eq. (7). In what follows, therefore, we focus on the low magnetic-field range ($B \lesssim 0.35$ T), where SdHOs remain virtually unaffected by the spin splitting. In the range of T_e encompassed in the present study, μ_q is independent of the temperature, since the mobility is limited predominantly by the impurity scattering and the contribution from the electron-phonon scattering is negligibly small.^{26,27} This allows us to use the same value of μ_q deduced here in the analysis of the data taken at higher I_0 .

Substituting $\mu_q = 4.1$ m²/(V s) and using T_e as the fitting parameter, the fitting of Eq. (7) to the amplitudes of the SdHOs extracted from R_L and R_H allows us to deduce the electron temperatures T_L and T_H , as exemplified in Fig. 3(c). As mentioned above, the fitting is performed

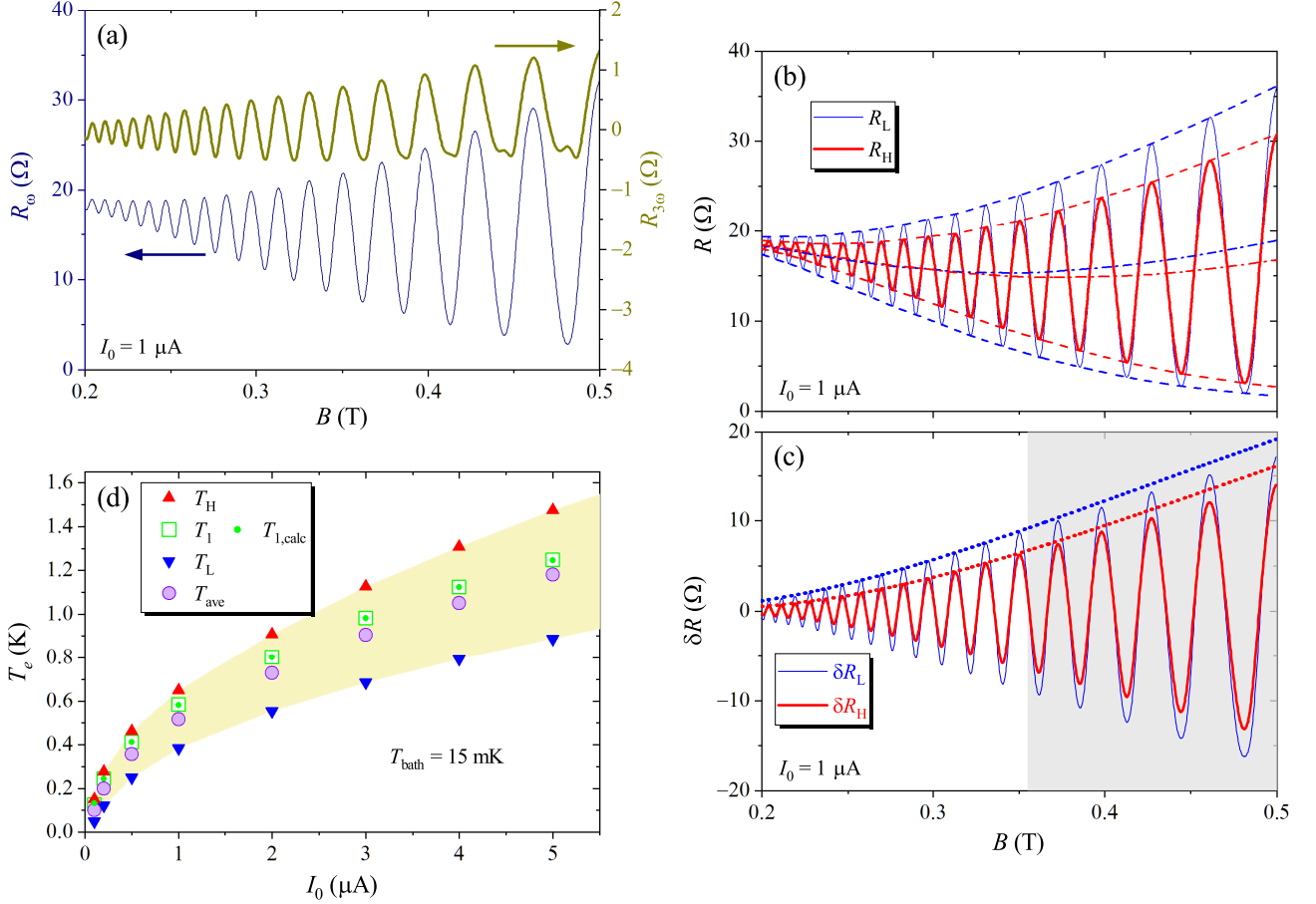


FIG. 3. (a)-(c) Illustration of the derivation of T_L and T_H from R_ω and $R_{3\omega}$, taking the case for $I_0 = 1 \mu\text{A}$ as an example. (a) R_ω (thin line, left axis) and $R_{3\omega}$ (thick line, right axis). (b) R_L (thin solid line) and R_H (thick solid line) calculated by Eq. (6) from R_ω and $R_{3\omega}$ in (a). Dashed lines represent the upper (R_{up}) and lower (R_{lw}) envelopes of the SdHOs and the dotted-dashed lines are their averages $R_{\text{bg}} = (R_{\text{up}} + R_{\text{lw}})/2$, which are taken as the slowly-varying backgrounds. (c) The oscillatory parts δR_L (thin solid line) and δR_H (thick solid line) obtained by subtracting the corresponding background R_{bg} from R_L and R_H in (b). The dotted lines represent Eq. (7) with $T_e = T_L = 0.39 \text{ K}$ and $T_e = T_H = 0.65 \text{ K}$, which reproduce the amplitude of δR_L and δR_H , respectively, below $\sim 0.35 \text{ T}$. Shaded area indicates the range of the magnetic field where the amplitudes are reduced due to the effect of incipient spin-splitting. (d) T_L and T_H for various values of I_0 , obtained by following the procedure exemplified in (a)-(c). The average temperature, $T_{\text{ave}} = (T_L + T_H)/2$, and the temperature obtained from the analysis of the SdHOs in R_ω , T_1 , are also plotted. T_1 shows good agreement with $T_{1,\text{calc}}$ (indicated by the small dots) calculated by Eq. (8) from T_L and T_H .

in the limited magnetic field range ($B \lesssim 0.35 \text{ T}$). Here again, we can see slight deviation caused by the incipient incomplete spin splitting at higher magnetic fields [the shaded region in Fig. 3(c)].

In Fig. 3(d), we compile T_L and T_H obtained for various values of I_0 ranging from 100 nA to $5 \mu\text{A}$. The figure, representing one of the highlights in the present study, shows how the average temperature $T_{\text{ave}} = (T_L + T_H)/2$ and the temperature increment $\Delta T = T_H - T_L$ increase with I_0 . A more conventional way to estimate the electron temperature of a 2DEG heated by a current is to perform the analysis of the amplitude of SdHOs directly on R_ω .^{9,18,28} We have applied the same analysis described above to the SdHOs in R_ω . The resulting electron temperature T_1 , also plotted in Fig. 3(d), reveals that the

conventional method yields temperatures slightly higher than T_{ave} . For more quantitative account of T_1 , we recall the relation between R_ω and R_L , R_H , Eq. (5), which leads to the relation between the temperatures,

$$A \left(\frac{T_1}{T_c} \right) = \frac{3A(T_H/T_c) + A(T_L/T_c)}{4}. \quad (8)$$

In Fig. 3(d), we also plot values of T_1 numerically calculated with Eq. (8) from T_L and T_H , which show excellent agreement with T_1 obtained from the direct analysis of R_ω .

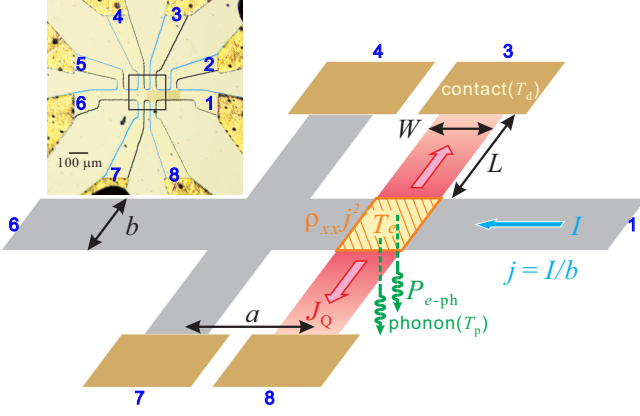


FIG. 4. Schematic illustration of the thermal flow in a Hall bar device. $\rho_{xx}j^2$: Joule heating per area by the current density $j = I/b$. J_Q : thermal flux due to diffusion into the contact pads. P_{e-ph} : power per area transferred to the lattice via the electron-phonon interaction. Inset: Optical micrograph of the Hall bar device used in the present study. The main panel corresponds to the area enclosed by the rectangle.

D. Thermal conductivity of a 2DEG

The response of the temperature to the Joule heating drawn out in Sec. III C allows us to roughly estimate the thermal conductivity κ_{xx} of the 2DEG. We consider a simple Hall-bar device having the main channel with the width b and the voltage arms with the width W and the length L , as schematically depicted in Fig. 4. The current I passing through the main channel introduces Joule heat $\rho_{xx}j^2$ per area to the 2DEG residing in the main channel, where ρ_{xx} is the resistivity of the 2DEG and $j = I/b$ is the current density. Now we focus on the hatched area in Fig. 4, namely, the part of the main-channel area in direct connection to the voltage arms. The heat deposited to this area by the Joule heating, $\rho_{xx}j^2bW$, is lost by diffusion through the voltage arms into the electric contact (J_Q) or by being imparted to the lattice via the electron-phonon interaction (P_{e-ph}).²⁹

In a recent publication,³⁰ the present authors have shown that the thermal flux from the high-temperature end (T_s) to the low-temperature end (T_d) along the length of the rectangular 2DEG area (length L and width W), when placed in a magnetic field, is given by

$$J_Q(T_s, T_d) = \frac{K_{xx}}{\cos \delta} \frac{\alpha}{S(\delta, \alpha)} \frac{T_s^2 - T_d^2}{2}, \quad (9)$$

where $\alpha = W/L$ is the aspect ratio, $\delta = \arctan(\sigma_{yx}/\sigma_{xx})$ is the Hall angle with σ_{yx} and σ_{xx} the Hall conductivity and the diagonal conductivity, respectively,

$$S(\delta, \alpha) \equiv \int_0^1 \cos \left\{ 4\delta \sum_{n=1}^{\infty} \frac{\sin[(2n-1)\pi\xi]}{(2n-1)\pi} \operatorname{sech} \left[(2n-1) \frac{\alpha\pi}{2} \right] \right\} d\xi, \quad (10)$$

and

$$K_{xx} \equiv \kappa_{xx}/T_e. \quad (11)$$

In the derivation of Eq. (9), we assumed that K_{xx} is independent of T_e , which is good approximation for 2DEGs at low temperatures ($T_e \lesssim 1$ K).³⁰ We have also shown that $S(\delta, \alpha) \simeq \alpha$ for $\alpha \lesssim 0.5$ in a moderate-to-high magnetic field where δ approaches $\pi/2$ in a high-mobility 2DEG, and thus $J_Q(T_s, T_d)$ becomes independent of α ,

$$J_Q(T_s, T_d) \simeq \frac{K_{xx}}{\cos \delta} \frac{T_s^2 - T_d^2}{2}. \quad (12)$$

This allows us to apply Eq. (12), to good approximation, to a voltage arm of a Hall-bar device even if the arm is not of rectangular shape, so long as the arm is long enough. The Hall-bar device used in the present study is shown in the inset of Fig. 4. Although the arms retain rectangular shape only for a certain distance from the main channel, the small aspect ratio α throughout the arms justifies, to a certain degree, the use of the approximation Eq. (12).

The power per area transferred from the 2DEG at the temperature T_e to the phonons at the temperature T_p is written as^{15,30,31}

$$P_{e-ph}(T_e, T_p) = P_l^{\text{df}}(T_e, T_p) + P_l^{\text{pz}}(T_e, T_p) + 2P_t^{\text{pz}}(T_e, T_p), \quad (13)$$

with

$$P_s^r(T_e, T_p) = \Pi_s^r(T_e) - \Pi_s^r(T_p), \quad (14)$$

where the deformation-potential coupling and the piezoelectric coupling are denoted by $r = \text{df}$ and pz , respectively, and $s = l$ and t represent the longitudinal and the transverse modes, respectively. The functions^{15,31} $\Pi_s^r(T)$ are given by³²

$$\Pi_l^{\text{df}}(T) = \frac{e^2 D^2 v_l a_B^{*2}}{64\sqrt{2}\pi^{\frac{5}{2}} \mu_B^{*2} \rho} \left(\frac{k_B T}{\hbar v_l} \right)^7 \frac{G_l^{\text{df}}(n_e, T)}{\sqrt{n_e}} \quad (15a)$$

$$\Pi_s^{\text{pz}}(T) = \frac{e^4 h_{14}^2 v_s a_B^{*2}}{64\sqrt{2}\pi^{\frac{5}{2}} \mu_B^{*2} \rho} \left(\frac{k_B T}{\hbar v_s} \right)^5 \frac{G_s^{\text{pz}}(n_e, T)}{\sqrt{n_e}} \quad (15b)$$

($s = l, t$).

The material parameters for GaAs in Eq. (15) used in the calculations below are as follows: the deformation potential $D = -8.33$ eV,³³ the piezoelectric constant $h_{14} = 1.2 \times 10^9$ V/m,³⁴⁻³⁶ the longitudinal sound velocity $v_l = 5.14 \times 10^3$ m/s,^{35,36} the transverse sound velocity $v_t = 3.04 \times 10^3$ m/s,^{35,36} the mass density $\rho = 5.3$ g/cm³,³⁷ the effective Bohr radius $a_B^* = 10.4$ nm,³¹ and $\mu_B^* \equiv e\hbar/(2m^*) = 0.864$ meV/T with the effective mass $m^* = 0.067m_e$,³⁸ where m_e is the bare electron mass. The dimensionless functions^{15,31} $G_s^r(n_e, T)$ are detailed in the Appendix.

By balancing the incoming and outgoing thermal flux at the hatched area in Fig. 4, we have

$$\rho_{xx}j^2bW = 2J_Q(T_e, T_d) + P_{e-ph}(T_e, T_p)bW, \quad (16)$$

from which we arrive at the expression for the thermal conductivity

$$\kappa_{xx} = K_{xx}T_e = bW \frac{T_e}{T_e^2 - T_d^2} \cos \delta [\rho_{xx}j^2 - P_{e-ph}(T_e, T_p)]. \quad (17)$$

To proceed further, it is necessary to make several assumptions regarding the temperatures to be substituted into Eq. (17). As can be seen in Fig. 1, T_L corresponds to the electron temperature of the 2DEG at the moment the Joule heating vanishes. Therefore, we consider that T_L also represents the lattice temperature of the part of the substrate in direct contact with the 2DEG, namely, $T_p = T_L$; the thin layer buried in the substrate, located in the vicinity of GaAs/AlGaAs heterojunction and hosting the 2DEG having the thickness of the wavefunction ~ 10 nm, can be heated, via the electron-phonon interaction, to a lattice temperature higher compared to the rest of the substrate. On the other hand, we assume that the temperature of the electrical contact is the same as the bath temperature, $T_d = T_{\text{bath}}$, since the contact pad made of a thin metallic (AuGeNi) film has a granular surface (see the inset to Fig. 4) and therefore expected to be in good thermal contact with the surrounding helium liquid,³⁰ in marked contrast with the thin slab buried in the GaAs substrate. Taking the average temperature T_{ave} as resulting from the root mean square value of the Joule heating, we substitute $T_e = T_{\text{ave}}$ and $\rho_{xx}j^2 = R_{\text{bg,ave}}I_0^2/(ab)$ into Eq. (17), where we used $R_{\text{bg,ave}} = (R_{L,\text{bg}} + R_{H,\text{bg}})/2$, the average of the backgrounds of R_L and R_H [exemplified by the dotted-dashed lines in Fig. 3 (b)],³⁹ to evaluate the resistivity $\rho_{xx} = R_{\text{bg,ave}}b/a$ responsible for the Joule heating,⁴⁰ with a representing the distance between the voltage arms employed for the measurement of R_{xx} (see Fig. 4). We also used the same ρ_{xx} along with the semiclassical Hall resistivity⁴¹ $\rho_{xy} = B/(n_e e)$ to calculate the Hall angle $\delta = \arctan(\rho_{xy}/\rho_{xx})$. The dimensions of the Hall-bar device in the present study are $a = 62 \mu\text{m}$, $b = 52 \mu\text{m}$, and $W = 32 \mu\text{m}$.

In the main panel of Fig. 5, we plot κ_{xx} thus calculated for various values of I_0 at $B = 0.3$ T as a function of $T_e = T_{\text{ave}}$. We also plot, for comparison, the thermal conductivity calculated from the electrical conductivity $\sigma_{xx} = \rho_{xx}/(\rho_{xx}^2 + \rho_{xy}^2)$ employing the Wiedemann-Franz law, valid at low temperatures,⁴²

$$\kappa_{xx}^{\text{WF}} = L_0 T_e \sigma_{xx}, \quad (18)$$

where $L_0 = \pi^2 k_B^2 / (3e^2) = 2.44 \times 10^{-8} \text{ V}^2/\text{K}^2$ is the Lorenz number. Slight deviation of the κ_{xx}^{WF} from the simple linear- T behavior (indicated by the dashed line) is due to the small variation of σ_{xx} with I_0 . We can see that κ_{xx} obtained by Eq. (17) roughly follows the increasing trend of κ_{xx}^{WF} with T_e . Comparison with the Wiedemann-Franz law can be made more clearly in the inset to Fig. 5, in which we plot the effective Lorenz number

$$L_{\text{eff}} \equiv \frac{\kappa_{xx}}{T_e \sigma_{xx}} = \frac{K_{xx}}{\sigma_{xx}} \quad (19)$$

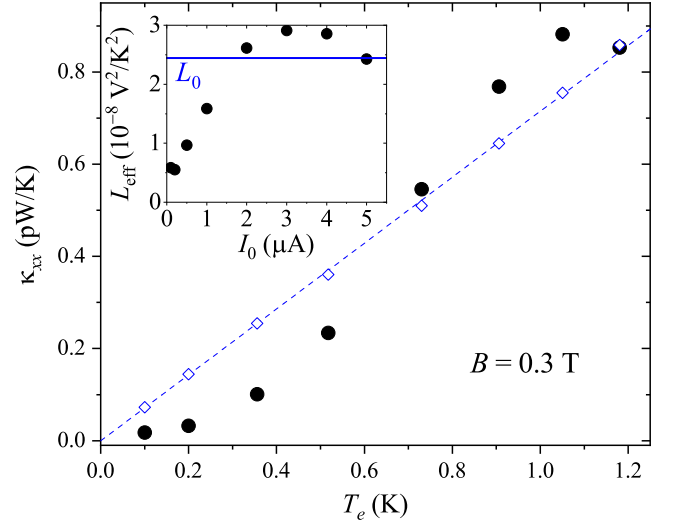


FIG. 5. Thermal conductivity κ_{xx} calculated by Eq. (17) with $T_e = T_{\text{ave}}$ at $B = 0.3$ T (solid circles). κ_{xx}^{WF} calculated by the Wiedemann-Franz law, Eq. (18), is plotted by open diamonds. (Dashed line is an eye guide). Inset: effective Lorenz number L_{eff} given by Eq. (19) plotted against I_0 . The horizontal line indicates the value L_0 corresponding to the Wiedemann-Franz law.

against I_0 . Although L_{eff} coincides with the Wiedemann-Franz value L_0 within an order of magnitude, deviations are apparent especially at low I_0 (low T_e) region. We consider that the low- T_e deviation mainly results from the assumption $T_d = T_{\text{bath}}$ mentioned above, suggesting the possibility that the electric contacts are heated above the temperature of the surrounding helium bath by the inflowing thermal flux. Slight increase in T_d let the κ_{xx} approach κ_{xx}^{WF} by diminishing the denominator in Eq. (17) when T_e is low and relatively close to T_d . With the increase of T_e , the role of the term $P_{e-ph}(T_e, T_p)$ in Eq. (17) becomes acceleratingly important, since it contains the terms varying as T_e^5 or T_e^7 . At higher T_e , therefore, the accuracy of the deduced κ_{xx} is severely limited by the preciseness of the values of D and h_{14} , which exhibit relatively wide variations among the literature^{9,33–38,43–45} ($|D| = 6.7\text{--}11 \text{ eV}$, $h_{14} = 1.2\text{--}1.45 \times 10^9 \text{ V/m}$). We have chosen the values of D and h_{14} noted above, rather arbitrarily, to achieve the fairly good agreement between κ_{xx} and κ_{xx}^{WF} shown in Fig. 5. Considering that a rather simplistic model, represented by Fig. 4 and Eq. (12),⁴⁶ is employed for the analysis, we take the obtained values of κ_{xx} to be acceptably close to the expected values κ_{xx}^{WF} . We stress that the procedure described here provides a handy method to roughly estimate the thermal conductivity using only a simple experimental setup for standard ac lock-in resistance measurement and a standard Hall bar device.

So far, we have employed Eq. (17) to deduce κ_{xx} using material parameters taken from the literature and assuming the values of the relevant temperatures. Conversely, one can, in principle, employ Eq. (17) to esti-

mate D , h_{14} and T_d by postulating that κ_{xx}^{WF} gives the correct value of the thermal conductivity. By first determining T_d from lower temperature region and then by performing the fitting employing D and h_{14} as fitting parameters, we can let κ_{xx} in Eq. (17) reproduce κ_{xx}^{WF} within $\sim 10\%$ by taking $T_d(\text{K}) = (1/2)\{T_e(\text{K}) - 0.3222 - \sqrt{0.01384 + [T_e(\text{K}) - 0.3222]^2}\} + 0.3222$,⁴⁷ $h_{14} = 1.44 \times 10^9$ V/m, and $D = 0$ (namely, by neglecting the deformation-potential contribution). Note, however, that the reliability of these values is severely limited by the oversimplified model mentioned above.

IV. CONCLUSIONS

We have shown that the Joule heating of a GaAs/AlGaAs 2DEG by an ac current with the angular frequency ω , accompanied by the oscillating electron temperature T_e having the angular frequency 2ω , can be monitored by detecting the fundamental (ω) and the third-harmonic (3ω) contents of the resulting voltage drop. We have deduced the highest (T_H) and the lowest (T_L) temperatures of the oscillating T_e for various values of the heating current. Employing the temperature response to the Joule heating thus acquired, we have further drawn out the thermal conductivity κ_{xx} of the 2DEG, with the aid of the simple formula we have deduced in a recent publication³⁰ modeling the thermal flux through the voltage arms, and the well-known formulas for the power per area transferred from the 2DEG to the lattice system.^{15,30,31} The resulting κ_{xx} is found to be roughly in agreement with the thermal conductivity estimated from the electrical conductivity via the Wiedemann-Franz law. The procedure we have taken here to deduce κ_{xx} , corresponding to 2D analog of the 3ω method, provides us with a convenient method to roughly estimate the thermal conductivity using only a simple Hall-bar sample and the conventional experimental setup for the resistance measurement by the ac lock-in technique.

SUPPLEMENTARY MATERIAL

See the Supplementary Material for I. R_ω and $R_{3\omega}$ taken with various frequencies at $I_0 = 1 \mu\text{A}$, II. R_ω and $R_{3\omega}$ taken at various temperatures at $I_0 = 10 \text{ nA}$, III. measurements and analyses similar to those shown in Sec. III of the main text but performed at an elevated bath temperature $T_{\text{bath}} = 600 \text{ mK}$, and IV. procedure for deducing the quantum mobility μ_q .

ACKNOWLEDGMENTS

This work was supported by JSPS KAKENHI Grants No. JP20K03817 and No. JP19H00652.

Appendix: The dimensionless functions $G_s^r(n_e, T)$

In this Appendix, we present the detailed description of the dimensionless functions $G_s^r(n_e, T)$ ($r = \text{df, pz}$ and $s = l, t$) in Eq. (15) for completeness. The functions are written as^{15,31}

$$G_s^r(n_e, T) \equiv \frac{1}{\pi} \int_{-\infty}^{\infty} d\zeta |F(q_{Ts}\zeta)|^2 \times \int_0^{\kappa_F} \frac{d\xi}{\sqrt{1 - (\xi/\kappa_F)^2}} \frac{g_s^r(\xi, \zeta)}{e^{\sqrt{\xi^2 + \zeta^2}} - 1} \frac{1}{H^2(q_{Ts}\zeta)} \quad (\text{A.1})$$

with

$$F(q_z) = \int dz |\Phi(z)|^2 e^{iq_z z}, \quad (\text{A.2})$$

and

$$H(q_{\parallel}) = \iint dz_1 dz_2 |\Phi(z_1)|^2 |\Phi(z_2)|^2 e^{-q_{\parallel}|z_1 - z_2|}, \quad (\text{A.3})$$

where q_z and q_{\parallel} are the components of the phonon wavevector perpendicular and parallel to the 2DEG plane, respectively, $\Phi(z)$ represents the envelope of the 2DEG wavefunction in the z direction, and $\kappa_F \equiv 2k_F/q_{Ts}$, $\xi \equiv q_{\parallel}/q_{Ts}$, $\zeta \equiv q_z/q_{Ts}$ with $q_{Ts} \equiv k_B T/\hbar v_s$ representing the typical wavenumber of the acoustic phonons at the temperature T . The kernels $g_s^r(\xi, \zeta)$ in Eq. (A.1) are given by^{15,31}

$$g_l^{\text{def}}(\xi, \zeta) \equiv \xi^2(\xi^2 + \zeta^2)^{3/2}, \quad (\text{A.4})$$

$$g_l^{\text{pz}}(\xi, \zeta) \equiv \frac{9\xi^6\zeta^2}{2(\xi^2 + \zeta^2)^{5/2}}, \quad (\text{A.5})$$

and

$$g_t^{\text{pz}}(\xi, \zeta) \equiv \frac{8\xi^4\zeta^4 + \xi^8}{4(\xi^2 + \zeta^2)^{5/2}}. \quad (\text{A.6})$$

Noting that q_{Ts} is smaller than the inverse of the rms thickness $\sim 5 \text{ nm}$ of our 2DEG⁴⁸ in the temperature range $T_p < T_e \lesssim 1.2 \text{ K}$ encompassed in the present study, we can make an approximation $\Phi(z) \simeq \delta(z)$ and thus replace $|F(q_z)|$ and $H(q_{\parallel})$ in Eq. (A.1) by unity to good approximation.

AUTHOR DECLARATIONS

Conflict of Interest

The authors have no conflicts to disclose.

DATA AVAILABILITY

The data that support the findings of this study are available from the corresponding author upon reasonable request.

- ¹N. J. Appleyard, J. T. Nicholls, M. Y. Simmons, W. R. Tribe, and M. Pepper, "Thermometer for the 2D electron gas using 1D thermopower," *Phys. Rev. Lett.* **81**, 3491–3494 (1998).
- ²V. Venkatachalam, S. Hart, L. Pfeiffer, K. West, and A. Yacoby, "Local thermometry of neutral modes on the quantum Hall edge," *Nat. Phys.* **8**, 676–681 (2012).
- ³A. K. M. Wennberg, S. N. Ytterboe, C. M. Gould, H. M. Bozler, J. Klem, and H. Morkoç, "Electron heating in a multiple-quantum-well structure below 1 K," *Phys. Rev. B* **34**, 4409–4411 (1986).
- ⁴R. T. Syme, M. J. Kelly, and M. Pepper, "Direct measurement of the thermal conductivity of a two-dimensional electron gas," *J. Phys.: Condens. Matter* **1**, 3375–3380 (1989).
- ⁵M. Schmidt, G. Schneider, C. Heyn, A. Stemann, and W. Hansen, "Zero-field thermopower of a thin heterostructure membrane with a two-dimensional electron gas," *Phys. Rev. B* **85**, 075408 (2012).
- ⁶A. Mittal, R. G. Wheeler, M. W. Keller, D. E. Prober, and R. N. Sacks, "Electron-phonon scattering rates in GaAs/AlGaAs 2DEG samples below 0.5 K," *Surf. Sci.* **361**, 537 (1996).
- ⁷A. Mittal, "Quantum transport in semiconductor submicron structures," in *Quantum Transport in Semiconductor Submicron Structures*, edited by B. Kramer (Kluwer Academic, Dordrecht, 1996) Chap. 5, p. 303.
- ⁸M. Schmidt, G. Schneider, C. Heyn, A. Stemann, and W. Hansen, "Thermopower of a 2D electron gas in suspended AlGaAs/GaAs heterostructures," *J. Electron. Mater.* **41**, 1286–1289 (2012).
- ⁹K. Hirakawa and H. Sakaki, "Energy relaxation of two-dimensional electrons and the deformation potential constant in selectively doped AlGaAs/GaAs heterojunctions," *Appl. Phys. Lett.* **49**, 889–891 (1986).
- ¹⁰Y. Ma, R. Fletcher, E. Zaremba, M. D'Iorio, C. T. Foxon, and J. J. Harris, "Energy-loss rates of two-dimensional electrons at a GaAs/Al_xGa_{1-x}As interface," *Phys. Rev. B* **43**, 9033–9044 (1991).
- ¹¹E. Chow and H. P. Wei, "Experiments on inelastic scattering in the integer quantum Hall effect," *Phys. Rev. B* **52**, 13749–13752 (1995).
- ¹²N. Samkharadze, A. Kumar, M. J. Manfra, L. N. Pfeiffer, K. W. West, and G. A. Csáthy, "Integrated electronic transport and thermometry at millikelvin temperatures and in strong magnetic fields," *Rev. Sci. Instrum.* **82**, 053902 (2011).
- ¹³D. G. Cahill, "Thermal conductivity measurement from 30 to 750 K: the 3ω method," *Rev. Sci. Instrum.* **61**, 802–808 (1990).
- ¹⁴H. S. Carslaw and J. C. Jaeger, *Conduction of Heat in Solids* (Oxford University Press, Oxford, 1959).
- ¹⁵P. J. Price, "Hot electrons in a GaAs heterolayer at low temperature," *J. Appl. Phys.* **53**, 6863–6866 (1982).
- ¹⁶B. L. Gallagher, T. Galloway, P. Beton, J. P. Oxley, S. P. Beaumont, S. Thoms, and C. D. W. Wilkinson, "Observation of universal thermopower fluctuations," *Phys. Rev. Lett.* **64**, 2058–2061 (1990).
- ¹⁷S. Maximov, M. Gbordzoe, H. Buhmann, L. W. Molenkamp, and D. Reuter, "Low-field diffusion magnetothermopower of a high-mobility two-dimensional electron gas," *Phys. Rev. B* **70**, 121308 (2004).
- ¹⁸K. Fujita, A. Endo, S. Katsumoto, and Y. Iye, "Measurement of diffusion thermopower in the quantum Hall systems," *Physica E* **42**, 1030–1033 (2010).
- ¹⁹Note that the two approximations are basically independent and thus Eq. (3) remains good approximation as long as $|R_H - R_L|$ is small even if $T_H - T_L$ is not so small, as is the case in the measurements presented below. Strictly speaking, the oscillations in R affects the Joule heating, which, in turn, alters the oscillations in R . The resulting oscillations determined self-consistently inevitably contain higher harmonic terms. However, we neglect these higher-order effects, which are small when $|R_H - R_L|$ is small.
- ²⁰Since thermalization takes place via the electron-electron and the electron-phonon interactions, and the scattering times for these interactions are of the order of picoseconds⁴⁹ and nanoseconds,^{7,31} respectively, in the GaAs-based 2DEG at cryogenic temperatures, the thermal process examined in the present study can be considered to take place instantaneously in the timescale of the measurements. This is confirmed by the absence of the frequency dependence.
- ²¹Close inspection of the oscillation amplitudes reveals that the declining commences above $I_0 = 1, 2, 3$, and $4 \mu\text{A}$ in the magnetic-field region $B < 0.24 \text{ T}$, $0.24 \text{ T} < B < 0.31 \text{ T}$, $0.31 \text{ T} < B < 0.36 \text{ T}$, and $0.36 \text{ T} < B < 0.40 \text{ T}$, respectively.
- ²²P. T. Coleridge, "Small-angle scattering in two-dimensional electron gases," *Phys. Rev. B* **44**, 3793–3801 (1991).
- ²³A. Endo, S. Katsumoto, and Y. Iye, "Envelope of commensurability magnetoresistance oscillation in unidirectional lateral superlattices," *Phys. Rev. B* **62**, 16761–16767 (2000).
- ²⁴Since the sample, as well as the wires connected to the sample (several centimeters long at the connected end), is immersed in the mixture of the dilution fridge, and the current source is appropriately filtered before being connected to the wires, we believe that T_e is not substantially higher than T_{bath} . We also have ample experimental evidence, including the developing fractional quantum Hall states or SdH amplitudes, showing that T_e keeps going down while T_{bath} is cooled down to the base temperature. Note, however, that the following analysis is valid even if T_e is heated to slightly above T_{bath} , so long as $T_e \ll T_c$ and thus $A(T_e/T_c) \simeq 1$. The value of μ_q obtained by replacing $A(T_e/T_c)$ with 1 is virtually indistinguishable from that deduced in the main text.
- ²⁵A. Endo and Y. Iye, "The effect of oscillating fermi energy on the line shape of the Shubnikov-de Haas oscillation in a two-dimensional electron gas," *J. Phys. Soc. Jpn.* **77**, 064713 (2008).
- ²⁶W. Walukiewicz, H. E. Ruda, J. Lagowski, and H. C. Gatos, "Electron mobility in modulation-doped heterostructures," *Phys. Rev. B* **30**, 4571–4582 (1984).
- ²⁷J. H. Davies, *The physics of low-dimensional semiconductors* (Cambridge University Press, Cambridge, 1998).
- ²⁸R. Fletcher, J. J. Harris, C. T. Foxon, and R. Stoner, "Hot-electron temperatures of two-dimensional electron gases using both de Haas-Shubnikov oscillations and the electron-electron interaction effect," *Phys. Rev. B* **45**, 6659–6669 (1992).
- ²⁹The contribution of the heat capacity is totally negligible due to the extremely small electronic specific heat C_e of a 2DEG,⁵⁰ $C_e/T \sim 1 \times 10^{-9} \text{ J}/(\text{m}^2\text{K}^2)$ at $B \lesssim 0.3 \text{ T}$, and thus $\omega \int_{T_L}^{T_H} C_e dT \ll \rho_{xx} j^2, J_Q/(bW), P_{e\text{-ph}}$.
- ³⁰A. Endo, K. Fujita, S. Katsumoto, and Y. Iye, "Spatial distribution of thermoelectric voltages in a Hall-bar shaped two-dimensional electron system under a magnetic field," *J. Phys. Commun.* **3**, 055005 (2019).
- ³¹A. Endo, T. Kajioka, and Y. Iye, "Commensurability oscillations in the radio-frequency conductivity of unidirectional lateral superlattices: Measurement of anisotropic conductivity by coplanar waveguide," *J. Phys. Soc. Jpn.* **82**, 054710 (2013).
- ³²Strictly speaking, these formulas are for $B = 0$. In the low magnetic-field range we employed for the analysis, however, the Landau quantization only superposes small ripples on the energy-independent density of states (DOS) at $B = 0$, rather than transforming the DOS into separated discrete levels. We therefore consider these formulas to serve as good approximation.
- ³³C. G. Van de Walle, "Band lineups and deformation potentials in the model-solid theory," *Phys. Rev. B* **39**, 1871–1883 (1989).
- ³⁴K. Lee, M. S. Shur, T. J. Drummond, and H. Morkoç, "Low field mobility of 2-d electron gas in modulation doped Al_xGa_{1-x}As/GaAs layers," *J. Appl. Phys.* **54**, 6432–6438 (1983).
- ³⁵S. K. Lyo, "Low-temperature phonon-drag thermoelectric power in heterojunctions," *Phys. Rev. B* **38**, 6345–6347 (1988).
- ³⁶S. K. Lyo, "Magnetoelectric oscillations of the phonon-drag thermoelectric power in heterojunctions," *Phys. Rev. B* **40**, 6458–

- 6461 (1989).
- ³⁷J. S. Blakemore, "Semiconducting and other major properties of gallium arsenide," J. Appl. Phys. **53**, R123–R181 (1982).
- ³⁸S. Adachi, "GaAs, AlAs, and $\text{Al}_x\text{Ga}_{1-x}\text{As}$: Material parameters for use in research and device applications," J. Appl. Phys. **58**, R1–R29 (1985).
- ³⁹Note that $R_{L,\text{bg}}$ and $R_{H,\text{bg}}$ are almost the same in the area unaffected by the spin splitting. Their separation at higher magnetic fields is attributable to the differing effect of the spin splitting at different temperatures.
- ⁴⁰Noting that the amplitude of SdHOs is relatively small compared to the background in the magnetic-field range considered here, we neglected the variation of the Joule heating caused by SdHOs. Enhanced and reduced Joule heating at the maxima and the minima of the SdHOs, respectively, lead to the reduction and the enhancement of the amplitude. Both result in the downward shift of the resistance and therefore their net effect on the amplitude is, more or less, expected to be cancelled.
- ⁴¹Experimentally measured Hall resistivity exhibits the onset of quantum Hall plateaus, but the deviation from the semiclassical Hall resistivity is negligibly small in the magnetic-field range considered here.
- ⁴²The Wiedemann-Franz (WF) law is expected to be valid at $T \ll E_F/k_B$ for systems following the Boltzmann transport equations. Strictly speaking, the rapidly-varying oscillatory part of the SdH oscillations further requires $T \ll T_c$. In the present discussion, however, we consider the WF law only for the slowly-varying background. Unfortunately, we are unaware of experimental evidence for the WF law to be valid for GaAs-based 2DEGs in the temperature and the magnetic-field range considered in the present study. At $B = 0$ and $2K \lesssim T \lesssim 6K$, however, the WF law was experimentally confirmed in Ref. 4.
- ⁴³C. M. Wolfe, G. E. Stillman, and W. T. Lindley, "Electron mobility in high-purity GaAs," J. Appl. Phys. **41**, 3088–3091 (1970).
- ⁴⁴P. J. Price, "Low temperature two-dimensional mobility of a GaAs heterolayer," Surf. Sci. **143**, 145–156 (1984).
- ⁴⁵A. Çakan, C. Sevik, and C. Bulutay, "Strained band edge characteristics from hybrid density functional theory and empirical pseudopotentials: GaAs, GaSb, InAs and InSb," J. Phys. D: Appl. Phys. **49**, 085104 (2016).
- ⁴⁶We have neglected the heat transferred to the phonon from the arms for simplicity. The possible effect of non-rectangular shape of the arms, potentially leading to the deviation from Eq. (12), is also not seriously taken into consideration.
- ⁴⁷This formula is less reliable at $T_e \gtrsim 0.5$ K, where T_d is obtained by extrapolating the low-temperature values since the little dependence of κ_{xx} on T_d hindered us from deducing T_d directly.
- ⁴⁸A. Endo and Y. Iye, "Dependence of modulation amplitude on electron density in unidirectional lateral superlattices: The effect of the thickness of the two-dimensional electron gas," J. Phys. Soc. Jpn. **74**, 1792 (2005).
- ⁴⁹H. Fukuyama and E. Abrahams, "Inelastic scattering time in two-dimensional disordered metals," Phys. Rev. B **27**, 5976–5980 (1983).
- ⁵⁰W. Zawadzki and R. Lassnig, "Magnetization, specific heat, magneto-thermal effect and thermoelectric power of two-dimensional electron gas in a quantizing magnetic field," Surf. Sci. **142**, 225–235 (1984).

Joule heating and the thermal conductivity of a two-dimensional electron gas at cryogenic temperatures studied by modified 3ω method

Akira Endo,^{a)} Shingo Katsumoto, and Yasuhiro Iye

The Institute for Solid State Physics, The University of Tokyo, 5-1-5 Kashiwanoha, Kashiwa, Chiba 277-8581, Japan

I. FREQUENCY DEPENDENCE OF R_ω AND $R_{3\omega}$

We have performed the measurements of R_ω and $R_{3\omega}$ at frequencies $f = \omega/(2\pi)$ varying from 19 Hz to 93 Hz for all the heating current I_0 presented in the main text. Both R_ω and $R_{3\omega}$ were found to exhibit virtually no frequency dependence in this frequency range, as exemplified by Fig S1 for $I_0 = 1 \mu\text{A}$ (except for the slight deterioration of the signal-to-noise ratio at the frequencies close to the commercial line frequency 50 Hz). So far, we have limited ourselves to the real part (in-phase oscillations) of R_ω and $R_{3\omega}$, although the measurements have been performed simultaneously for the imaginary parts (out-of-phase oscillations) $R_{\omega,\text{out}}$ and $R_{3\omega,\text{out}}$ as well. Both $R_{\omega,\text{out}}$ and $R_{3\omega,\text{out}}$ showed slight frequency dependence. Unfortunately, however, the frequency dependence is mainly attributable to an artifact caused by parasitic capacitive coupling between the wires measuring the diagonal and the Hall resistances.¹ In order to correctly investigate the frequency dependence, it will be necessary to replace the electrical wires in our dilution-fridge probe to coaxial cables so that the capacitive coupling can be eliminated. Coaxial cables will also be beneficial to extend the measurements up to orders of magnitude higher frequency ranges.

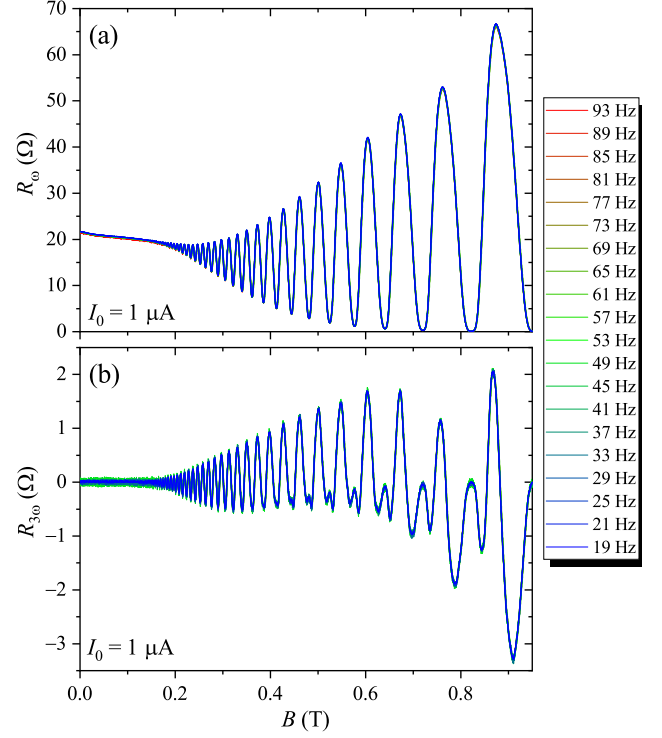


FIG. S1. The ω (a) and 3ω (b) components of the resistance R_ω and $R_{3\omega}$ for various values of the frequency, ranging from 19 Hz to 93 Hz, of the ac heating current with $I_0 = 1 \mu\text{A}$.

^{a)} akrendo@issp.u-tokyo.ac.jp

II. TEMPERATURE DEPENDENCE OF R_ω AND $R_{3\omega}$

We have measured the dependence of R_ω and $R_{3\omega}$ on the bath temperature $T_{\text{bath}} = 15\text{--}1000$ mK, employing a small current $I_0 = 10$ nA for which the heating effect is negligibly small. As shown in Fig. S2 (a), R_ω exhibits usual SdHO with the amplitude decreasing with increasing T_{bath} , bearing resemblance to the I_0 dependence shown in Fig. 2 (a) in the main text. The third-harmonic component $R_{3\omega}$, by contrast, does not show any discernible signal regardless of T_{bath} [Fig. S2 (b)] due to the absence of measurable heating effect.

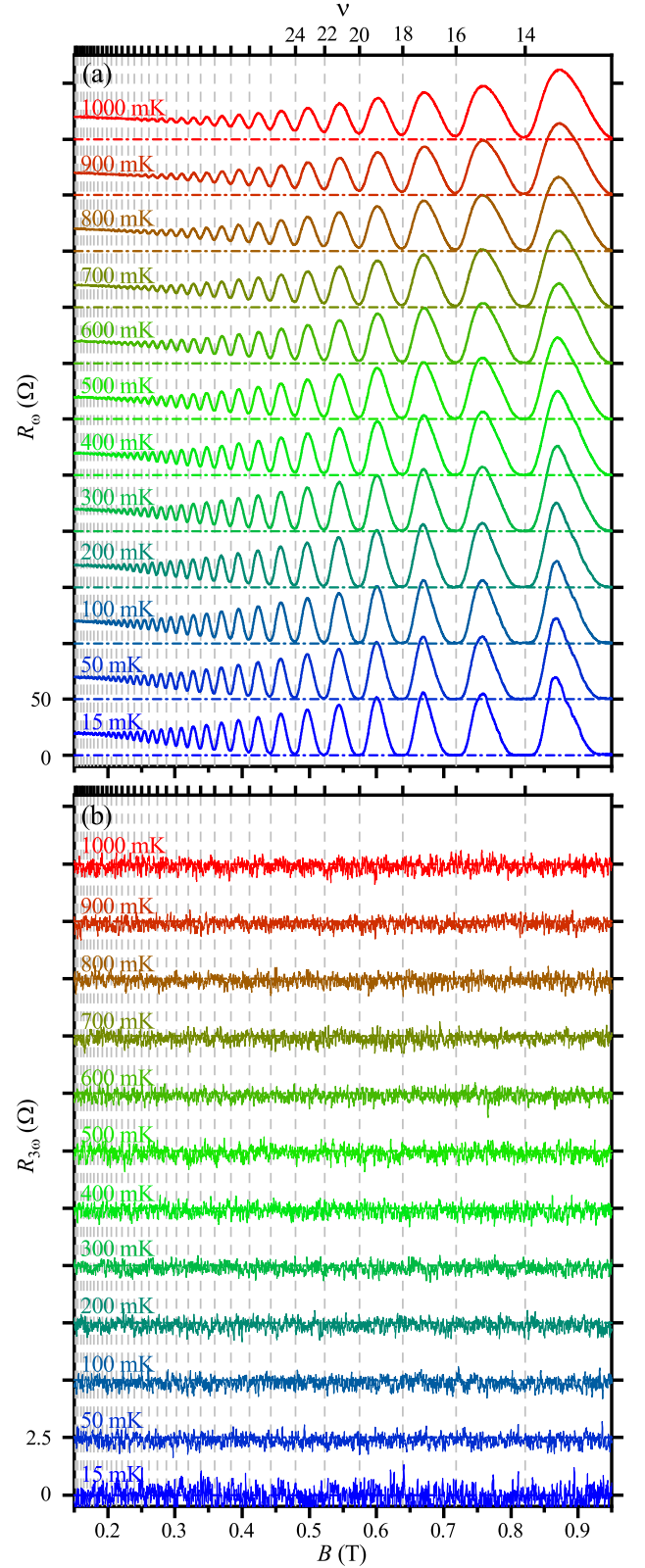


FIG. S2. The ω (a) and 3ω (b) components of the resistance R_ω and $R_{3\omega}$ measured at various bath temperatures T_{bath} noted in the figure. Traces are sequentially offset by 50 Ω and 2.5 Ω in (a) and (b), respectively, for clarity, with increasing T_{bath} . The vertical dashed lines and the horizontal dot-dashed lines indicate the positions of the even-integer fillings (top axis) and the zero for the corresponding trace, respectively. $I_0 = 10$ nA.

III. MEASUREMENTS AT AN ELEVATED BATH TEMPERATURE

We have repeated the measurements and analyses of R_ω and $R_{3\omega}$ described in section III of the main text, with the bath temperature $T_{\text{bath}} = 15$ mK (base temperature) replaced by an elevated temperature $T_{\text{bath}} = 600$ mK. In Fig. S3 (a) and (b), we plot R_ω and $R_{3\omega}$, respectively, measured at $T_{\text{bath}} = 600$ mK for various values of I_0 ranging from 10 nA to 5 μ A. Comparison of Fig. S3 (b) with its counterpart at $T_{\text{bath}} = 15$ mK [Fig. 2 (b) in the main text] reveals that the oscillation signals in $R_{3\omega}$ becomes smaller at the higher T_{bath} , especially at lower I_0 . This is mainly because the Joule heating by a smaller I_0 does not introduce enough temperature oscillations to be detected by $R_{3\omega}$ at the higher T_{bath} .

Following the analyses described in the main text, we calculated the highest (T_H) and the lowest (T_L) temperatures during a cycle of the temperature oscillations using R_ω and $R_{3\omega}$ shown in Fig. S3. These temperatures are plotted as a function of I_0 in Fig. S4, along with the average temperature T_{ave} , the temperature T_1 obtained from the conventional analysis of the SdHOs in R_ω , and $T_{1,\text{calc}}$ calculated from T_H and T_L using Eq. (8) in the main text. We can see that the temperature increment $\Delta T = T_H - T_L$ at $T_{\text{bath}} = 600$ mK is smaller, at low I_0 , than its counterpart at the base temperature shown in Fig. 3(d) in the main text, but gradually approaches the low- T_{bath} value with increasing I_0 .

The thermal conductivities κ_{xx} calculated with the temperatures in Fig. S4 using Eq. (17) in the main text, assuming $T_e = T_{\text{ave}}$ and $T_d = T_{\text{bath}}$, are plotted in Fig. S5 to be compared with Fig. 5 in the main text. The values of κ_{xx} calculated using the sample parameters taken from the literature noted in the main text are plotted by solid circles. Deviation at a higher T_e from the thermal conductivity κ_{xx}^{WF} calculated by the Wiedemann-Franz law becomes more prominent for the higher T_{bath} . We presume this to be mainly resulting from the uncertainty in the literature values of the electron-phonon coupling parameters D and h_{14} . Replacing the values of D and h_{14} with those obtained by the fitting at $T_{\text{bath}} = 15$ mK deduced in the main text ($D = 0$ and $h_{14} = 1.44 \times 10^9$ V/m), κ_{xx} , plotted with the open circles in Fig. S5, can be made closer to κ_{xx}^{WF} .

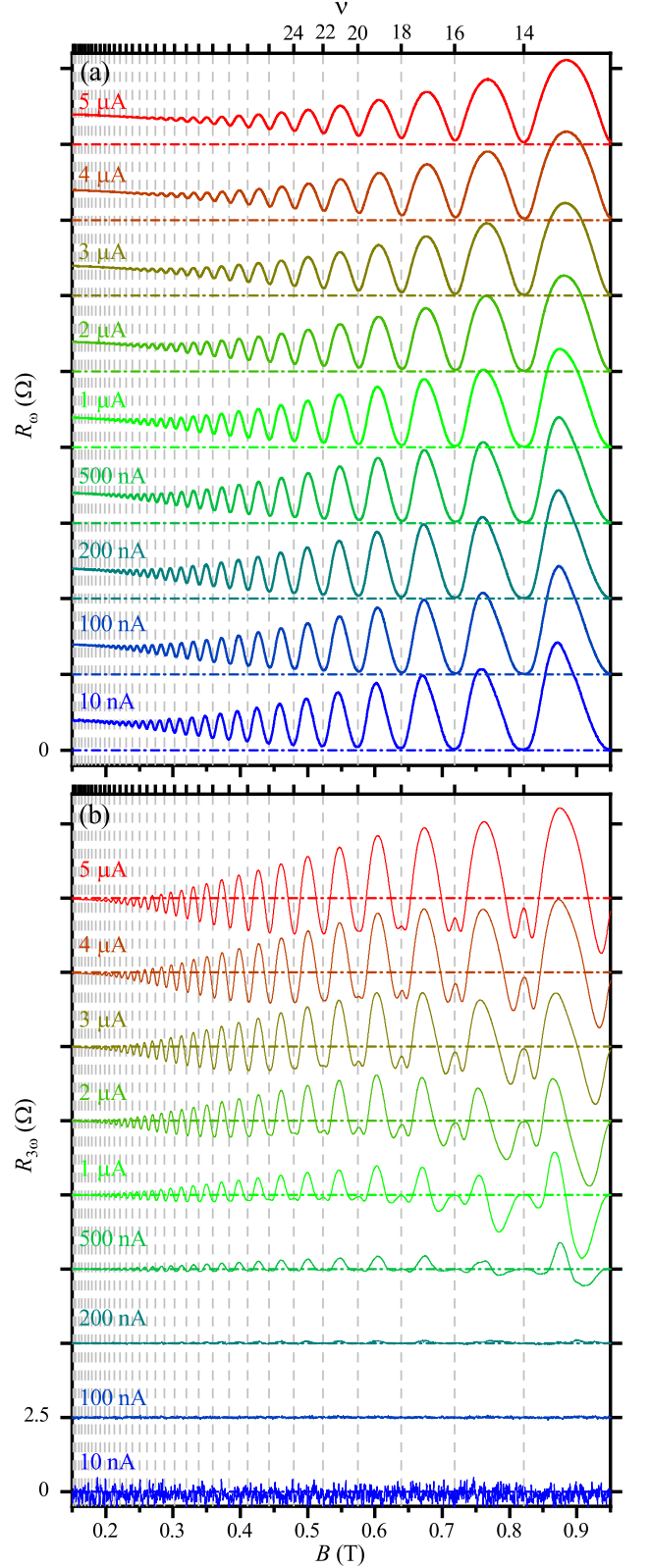


FIG. S3. The ω (a) and 3ω (b) components of the resistance R_ω and $R_{3\omega}$ measured at $T_{\text{bath}} = 600$ mK for various values of the heating current I_0 noted in the figures. Traces are sequentially offset by 50 Ω and 2.5 Ω in (a) and (b), respectively, for clarity, with increasing I_0 . The vertical dashed lines and the horizontal dot-dashed lines indicate the positions of the even-integer fillings (top axis) and the zero for the corresponding trace, respectively.

¹A. Endo, M. Kawamura, S. Katsumoto, and Y. Iye, “Magneto-transport of $\nu=3/2$ composite fermions under periodic effective magnetic-field modulation,” Phys. Rev. B **63**, 113310 (2001).

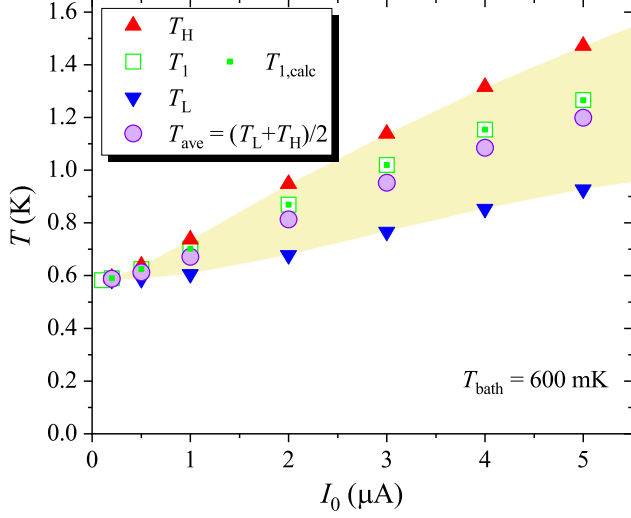


FIG. S4. T_L and T_H at $T_{\text{bath}} = 600$ mK for various values of I_0 , obtained from R_ω and $R_{3\omega}$ shown in Fig. S3 following

IV. DETERMINING THE QUANTUM MOBILITY μ_q

As described in IIIC of the main text, we extract the quantum mobility μ_q of our 2DEG from the decay of the SdH oscillations taken with the small current $I_0 = 10$ nA at the base temperature $T_{\text{bath}} = 15$ mK. The process is outlined in Fig. S6. As delineated in the main text, we first deduce the slowly varying background R_{bg} as an average of the upper (R_{up} , red dashed line) and the lower (R_{lw} , blue dashed line) envelopes [Fig. S6 (a)]. We then fit [Fig. S6 (b)] the amplitude of the oscillatory part δR_ω , obtained by subtracting the background, to Eq. (7), assuming $T_e = T_{\text{bath}}$, in the magnetic-field range $B \leq 0.35$ T, where the effect of the spin-splitting does not manifest itself in the resistance. We obtain $\mu_q = 4.1$ m²/(Vs) as the result of the fitting.

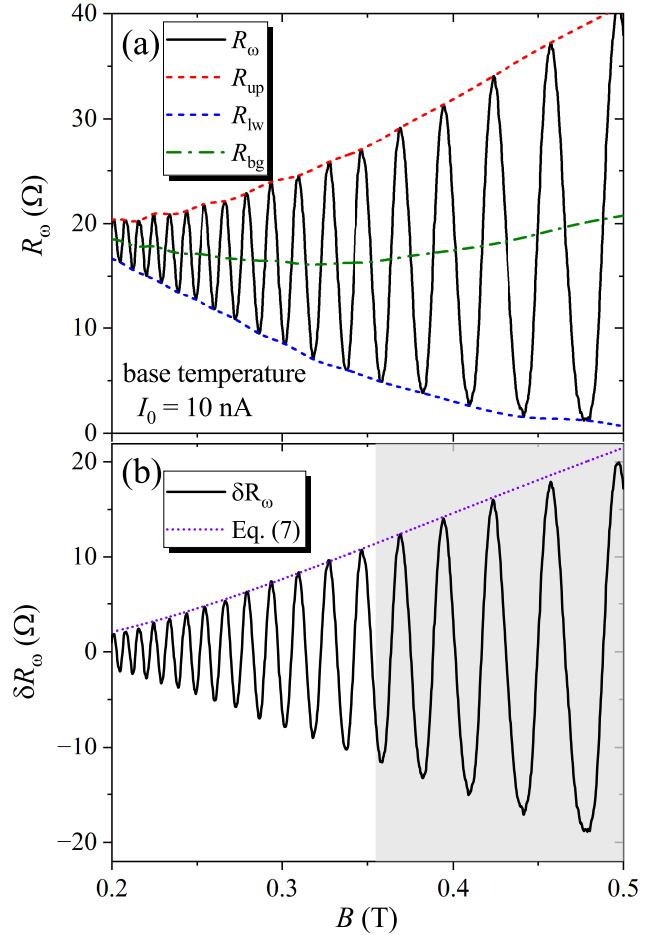


FIG. S5. Thermal conductivity κ_{xx} calculated by Eq. (14) in the main text with $T_e = T_{\text{ave}}$ at $B = 0.3$ T, using the parameters $D = -8.33$ eV and $h_{14} = 1.2 \times 10^9$ V/m (solid circles) or $D = 0$ and $h_{14} = 1.44 \times 10^9$ V/m (open circles). The values of κ_{xx}^{WF} calculated by the Wiedemann-Franz law, Eq. (18) in the main text, is plotted by open diamonds. (Dashed line is an eye guide). Inset: effective Lorenz number L_{eff} given by Eq. (19) in the main text plotted against I_0 . The horizontal line indicates the value L_0 corresponding to the Wiedemann-Franz law.

FIG. S6. (a) R_ω taken with $I_0 = 10$ nA at the base temperature [a part of the lowermost trace in Fig. 2 (a) in the main text, or in Fig. S2 (a)] (solid line), upper (R_{up}) and lower (R_{lw}) envelopes (dashed lines), and the slowly-varying background R_{bg} (dot-dashed line). (b) The oscillatory part $\delta R_\omega = R_\omega - R_{\text{bg}}$ (solid line) and the fitting of the amplitude to Eq. (7) in the main text (dotted line).